IV. OPTICAL AND INFRARED SPECTROSCOPY

Prof. C. H. Perry	W. J. Hakel	P. Lubitz
Dr. R. Geick	D. B. Hall	E. C. Reifenstein III
D. P. Athans		E. F. Young

A. WORK COMPLETED

The theses with the titles and authors listed below were submitted to the Department of Physics, M. I. T., May 1965, in partial fulfillment of the requirements for the degree of Bachelor of Science.

D. P. Athans, "Interferometric Far Infrared Analysis of Alkali Salts of Noble Metal Halide Complexes"

W. J. Hakel, "Infrared Reflectivity Spectra of Magnesium Germanide and Magnesium Stannide"

D. B. Hall, "Temperature Dependence of the Raman Effect of Barium Titanate"

P. Lubitz, "Frequency and Temperature Dependence of Reflectivity in Perovskites"

C. H. Perry

B. NORMAL MODES IN HEXAGONAL BORON NITRIDE

1. Introduction

The normal modes of lattice vibrations in hexagonal Boron Nitride have been investigated by means of infrared and Raman spectroscopy. In its hexagonal form, BN is a particularly interesting material among the III-V compounds. Many of these materials crystallize in the isotropic cubic zincblende-structure.[1] Others crystallize in the hexagonal wurzite structure[1] in which there is essentially a change of symmetry only as compared with the zincblende-structure, and not a change of nearest and next-nearest neighbors' distances. Thus the lattice vibrational properties of the wurtzite structure compounds are only slightly anisotropic.[2] While BN in its cubic form is similar to diamond, the hexagonal form is similar to graphite, with a hexagonal layer structure. Therefore its properties should be highly anisotropic.

2. Structure of Hexagonal BN

The structure of hexagonal BN has been investigated in the past with x-rays by Hassel[3] and Brager,[4] and more recently by Pease.[5] All investigators agree that the hexagonal unit cell is bimolecular and that the structure consists of layers of flat B_3N_3-hexagons with an interplanar spacing of c/2. According to the lattice parameters given by Pease,[5] the nearest neighbor's distances are $\frac{a}{\sqrt{3}} \approx 1.44\,\text{Å}$ in the hexagonal plane, and $\frac{c}{2} \approx 3.33\,\text{Å}$ parallel to the c-axis. There is, however, some disagreement concerning

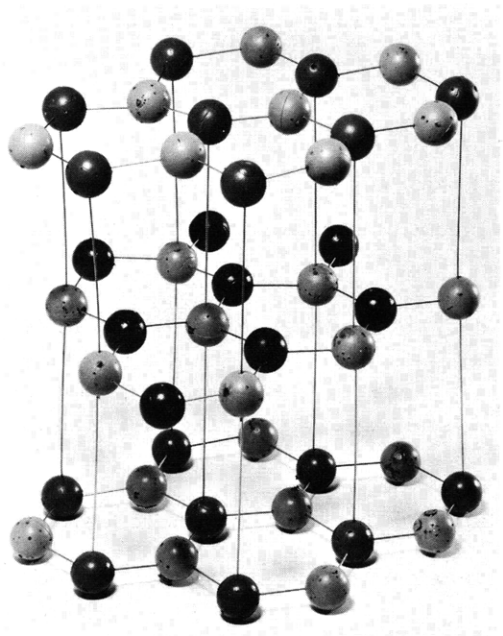

Fig. IV-1.
One of the possible graphitelike structures of BN (BN No. 1).

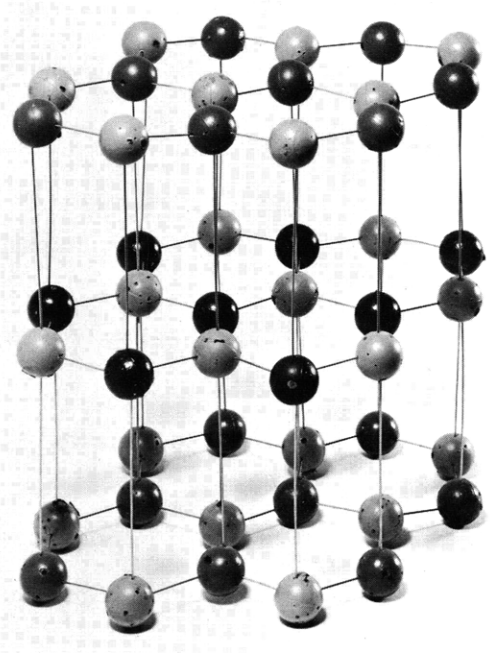

Fig. IV-2.
Structure of BN reported by Pease.[5] (BN No. 2)

the packing of the layers. Hassel and Brager reported a structure with B-ions and N-ions at sites occupied by carbon atoms in graphite. One of the possible graphitelike structures for BN is shown in Fig. IV-1. The ionic sites in the unit cell can be written as follows:

$$\text{B:}\quad 0; \qquad \tfrac{1}{3}(\vec{a}_1+2\vec{a}_2)+\tfrac{1}{2}\vec{a}_3$$

$$\text{N:}\quad -\tfrac{1}{3}(\vec{a}_1+2\vec{a}_2); \quad \tfrac{1}{2}\vec{a}_3$$

where $\vec{a}_1$, $\vec{a}_2$ and $\vec{a}_3$ are the lattice vectors. The point group of this lattice (BN No. 1) is D_{3h}. On the other hand, Pease reported a packing of the layers as shown in Fig. IV-2. In this case the ionic sites in the unit cell can be written

$$\text{B:}\quad +\tfrac{1}{3}(\vec{a}_1+2\vec{a}_2)+\tfrac{1}{4}\vec{a}_3; \quad -\tfrac{1}{3}(\vec{a}_1+2\vec{a}_2)-\tfrac{1}{4}\vec{a}_3$$

$$\text{N:}\quad -\tfrac{1}{3}(\vec{a}_1+2\vec{a}_2)+\tfrac{1}{4}\vec{a}_3; \quad +\tfrac{1}{3}(\vec{a}_1+2\vec{a}_2)-\tfrac{1}{4}\vec{a}_3.$$

The point group of this lattice (BN No. 2) is $D_{6h} = D_{3h} \times C_i$. Some of the symmetry operations are connected with nonprimitive translations.

Although the results of Pease seem to be more accurate, the data of the optical investigation will be discussed in terms of both structures in connection with group theoretical considerations. The important difference between the two structures is the center of symmetry in BN No. 2.

X-ray studies of our BN samples confirm Pease's results, but they also show that our samples are polycrystalline with some preference in the orientation of the c-axis.

3. Infrared and Raman Spectra

The reflectivity and the absorption coefficient of BN have been measured throughout the infrared spectral region from 300 cm^{-1} to 2000 cm^{-1} with linearly polarized light, with E parallel and perpendicular to the c-axis. The Raman scattering of BN was measured from 150 cm^{-1} to 2000 cm^{-1} frequency shift of the scattered light in the Stokes region.

The reflection spectra were analyzed by means of Kramers-Kronig analysis and by means of an optimum fit with a classical dispersion formula. The experimental data and the results of the analysis have been presented in a previous report.[6] Thus only the essential final results are repeated here.

$E \parallel c$

$\epsilon_\infty = 4.10$ $\quad \epsilon_o = 5.09$

$\omega_{t1} = 783\ cm^{-1}$ $\quad \omega_{\ell 1} = 828\ cm^{-1}$ $\quad s_1 = 572\ cm^{-1}$ $\quad \gamma_1 = 8.0\ cm^{-1}$

$\omega_{t2} = 1510\ cm^{-1}$ $\quad \omega_{\ell 2} = 1595\ cm^{-1}$ $\quad s_2 = 1020\ cm^{-1}$ $\quad \gamma_2 = 80.0\ cm^{-1}$

$E \perp c$

$\epsilon_\infty = 4.95$ $\quad \epsilon_o = 7.04$

$\omega_{t1} = 767\ cm^{-1}$ $\quad \omega_{\ell 1} = 778\ cm^{-1}$ $\quad s_1 = 351\ cm^{-1}$ $\quad \gamma_1 = 35.0\ cm^{-1}$

$\omega_{t2} = 1367\ cm^{-1}$ $\quad \omega_{\ell 2} = 1610\ cm^{-1}$ $\quad s_2 = 1870\ cm^{-1}$ $\quad \gamma_2 = 29.0\ cm^{-1}$

Here, ϵ_∞ and ϵ_o are the high frequency and static dielectric constants, respectively, $\omega_{t\nu}$, $\omega_{\ell\nu}$, s_ν, and γ_ν are the transverse and longitudinal optical frequencies, the oscillator strength, and the damping constant of normal mode ν, respectively. (For further details of the notation used here, see our previous report.[6]) Furthermore, the reflection data for both directions of polarization exhibit a 2-phonon peak at 1540 cm^{-1}.

For Raman scattering, the sample was oriented with the c-axis parallel to the direction of propagation of the scattered light (See Fig. IV-3). The measurements were performed with incident radiation unpolarized and polarized parallel and perpendicular to

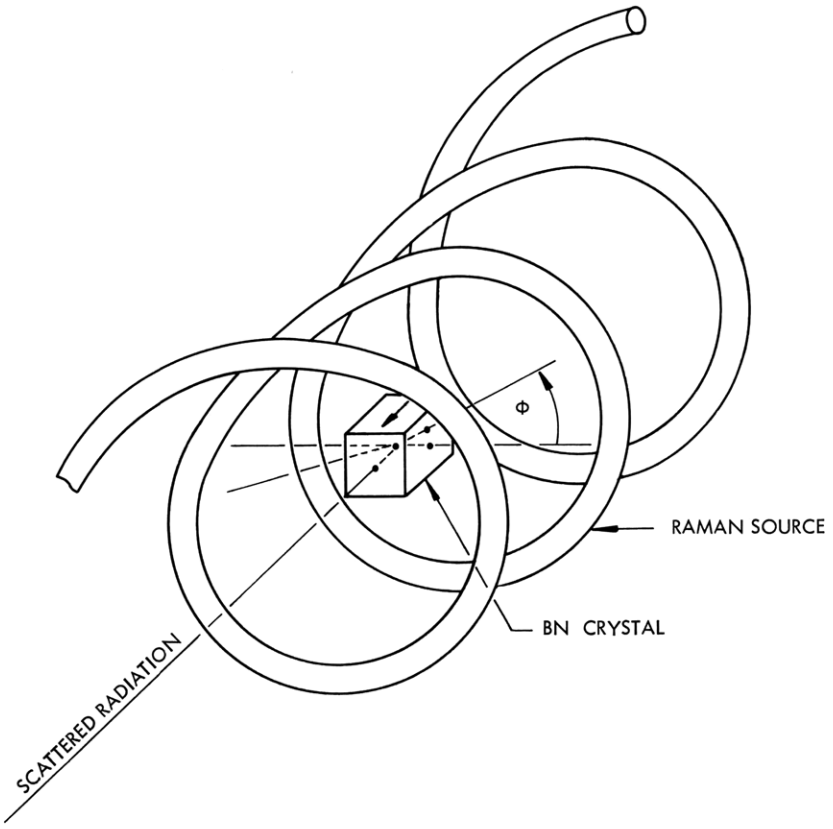

Fig. IV-3. Geometry of the arrangement used for Raman scattering.

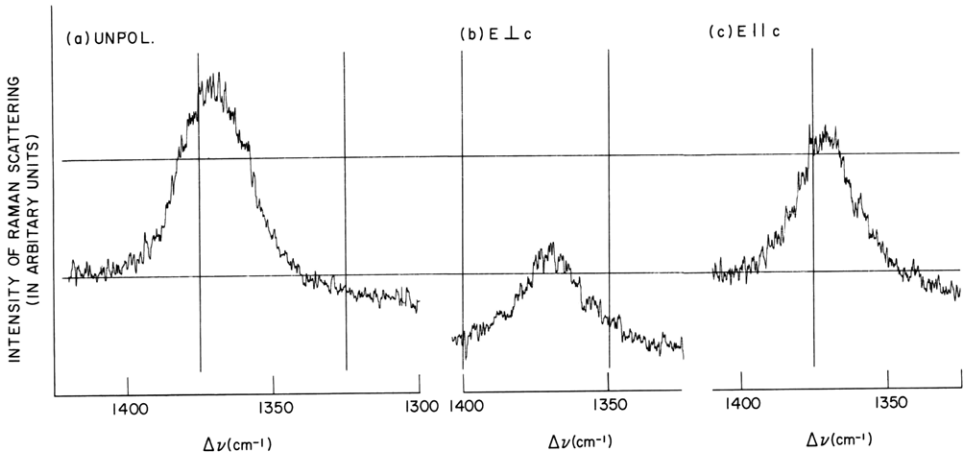

Fig. IV-4. Raman spectra of hexagonal BN.

the c-axis of the crystal. In all cases, one Raman line was found with ω_{Raman} = 1370 cm^{-1}, γ_{Raman} = 30 cm^{-1}, where γ_{Raman} is the half-width of the line (See Fig. IV-4). This line is ascribed to first-order Raman effect. There was no indication of second-order Raman peaks in the experimental results.

The absorption spectrum of BN exhibits major peaks near the infrared active eigenfrequencies, as determined from the reflection spectra (see Fig. IV-5). Furthermore,

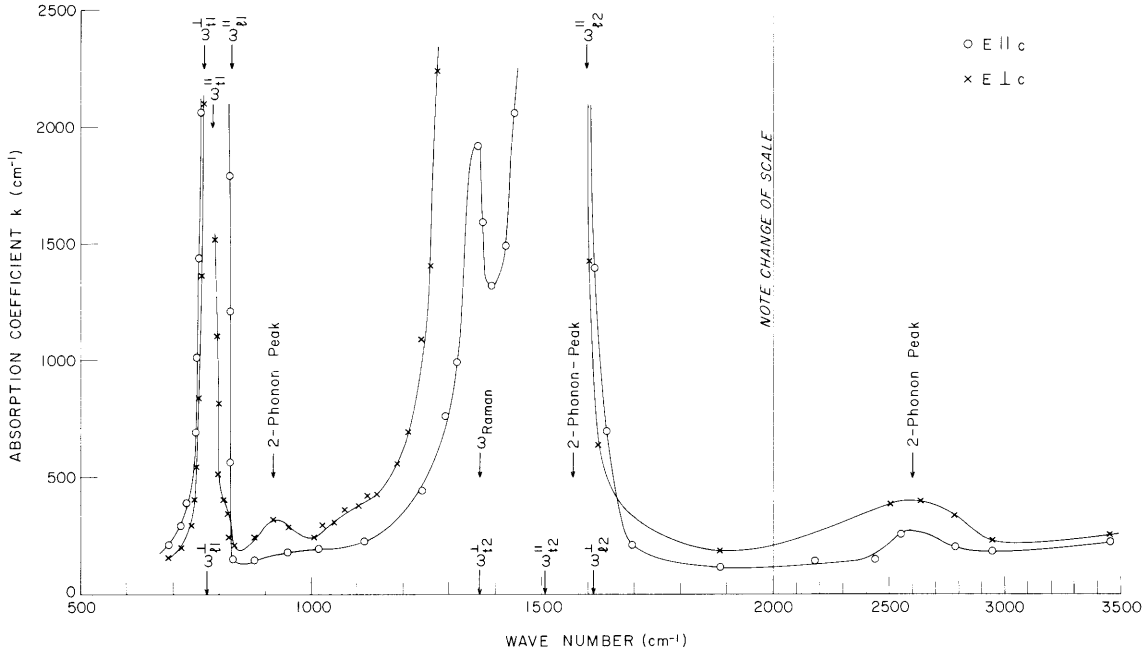

Fig. IV-5. Absorption coefficient of hexagonal BN for E ∥ c (x) and E ⊥ c (o). The arrows indicate also the frequencies determined from reflectivity and Raman data.

there are some minor peaks that are due to a high density of possible 2-phonon summation processes at 920 cm^{-1} and 2600 cm^{-1}. The 2-phonon peaks are more pronounced for E ⊥ c than for E ∥ c. An additional absorption peak arises for E ∥ c at the Raman frequency reported above. This peak is probably due to the interaction of the Raman mode with the nearby infrared active mode (cf. dispersion formula with interaction damping[6,7]). Also, the static dielectric constant has been determined independently at a frequency of 1 Mc/sec by capacity measurements: E ∥ c ϵ_o = 5.06; E ⊥ c ϵ_o = 6.85. These values agree quite well with those deduced from the reflectivity in the far infrared spectral region.

4. Group Theoretical Considerations

The species of the normal modes of the lattice vibrations and the resulting selection rules[8] will now be given for the two BN-lattices and compared with

the experimental results.

The irreducible representations for the normal modes near $\vec{k} = 0$ for BN No. 1 (without inversion symmetry) are:

3 acoustical modes	$E' + A_2''$
6 infrared active and Raman active optical modes	$3E'$
3 infrared active optical modes	$3A_2''$

In this case, three infrared active modes connected with reststrahlen bands should be found for each direction of polarization, as well as six Raman lines in pairs of two close together, since the longitudinal optical modes are also Raman-active but not infrared-active.

The irreducible representations for the normal modes near $\vec{k} = 0$ for BN No. 2 (with inversion symmetry) are:

3 acoustical modes	$A_{2u} + E_{1u}$
3 infrared active optical modes	$A_{2u} + E_{1u}$
4 Raman active optical modes	$2\,E_{2g}$
2 inactive optical modes	$2\,B_{1g}$

Under these conditions there should be, in the experimental results, only one reststrahlen band for each direction of polarization and two single Raman lines.

Now, in the infrared investigations we have found two active modes for each direction of polarization, a strong one and a weaker one. Though it could be that there is a third mode for each direction which has not been found, the results cannot be explained for a crystal without inversion symmetry. The highly anisotropic structure of BN requires highly anisotropic normal modes. Therefore the modes with slightly different frequencies have to be considered as one normal mode of the lattice. The weaker modes in the infrared spectra are then probably due to the misorientation in our polycrystalline sample. The small shift of their frequencies, as compared with the stronger modes, may be due to the angular dependence of the extraordinary waves.

The Raman data also clearly show that our sample has a symmetry center. Otherwise we should have found some indication of the longitudinal frequency in the vicinity of the Raman line. On the other hand, the Raman data for linearly polarized incident light indicate once more that there is considerable misorientation in our sample. Under the geometry of the Raman scattering, as given in Fig. IV-3, we can write

$$k_{\text{incident}} = k(\cos\theta\cos\phi, \cos\theta\sin\phi, \sin\theta)$$

$$k_{\text{scattered}} = k(\ 0\ ,\ 0\ ,\ 1\ )$$

Then the Raman intensity computed by means of the formula[9]

$$J = \text{const.} \sum_i \left[\sum_{\alpha,\beta} n_\alpha^i P_{\alpha\beta} E_\beta \right]^2$$

is for

$$E \parallel c \quad J = \text{const.}\ 2A^2 \sin^2\theta\, E^2$$

$$E \perp c \quad J = \text{const.}\ 2A^2 E^2,$$

with the symmetry of E_{2g} taken into account.[9] Since we are dealing, for the most part, with right-angle scattering ($\theta=0$), the intensity for $E \parallel c$ should be considerably smaller than for $E \perp c$ in contrast with the experimental results. The question about the second Raman frequency, which should be present in BN, is discussed in this report.

5. Normal Modes of BN

If we assume that the eigenfrequencies connected with the strong reststrahlen bands in the reflectivity represent the true eigenfrequencies of the lattice modes, we can list the following normal modes near $\vec{k} = 0$.

a) In plane

$\omega_{t1} = 1367\ \text{cm}^{-1}$ $\omega_{\ell 1} = 1610\ \text{cm}^{-1}$ (I. R.)

$\omega_{t2} = 1370\ \text{cm}^{-1}$ (Raman)

b) Out of plane

$\omega_{t3} = 783\ \text{cm}^{-1}$ $\omega_{\ell 3} = 828\ \text{cm}^{-1}$ (I. R.)

In order to discuss the accidental degeneracy of ω_{t1} and ω_{t2}, and the question of the second Raman frequency, a simple lattice model for the in-plane motion of the particles. was calculated. The forces assumed were a spring with force constant P between nearest neighbors in the plane and a weak interaction with constant force B between adjacent planes. The eigenfrequencies for in-plane motion with $k \approx 0$, according to this model, are:

$$\omega_1^2 = 0 \quad \text{(acoustical modes)}$$

$$\omega_2^2 = 2(P+B)\left(\frac{1}{m_B} + \frac{1}{m_N}\right) \quad \text{(I. R.-active)}$$

$$\omega_{3,4}^2 = (P+3B)\left(\frac{1}{m_B} + \frac{1}{m_N}\right) \pm \sqrt{(P+3B)^2\left(\frac{1}{m_B} - \frac{1}{m_N}\right)^2 + \frac{4}{m_B m_N}(P-B)^2}$$

(Raman-active)

Obviously for B « P there is $\omega_2^2 \approx \omega_3^2$. On the other hand, ω_4^2 depends strongly on B and will be very low compared with the other optical frequencies. The eigenvectors show this behavior more clearly:

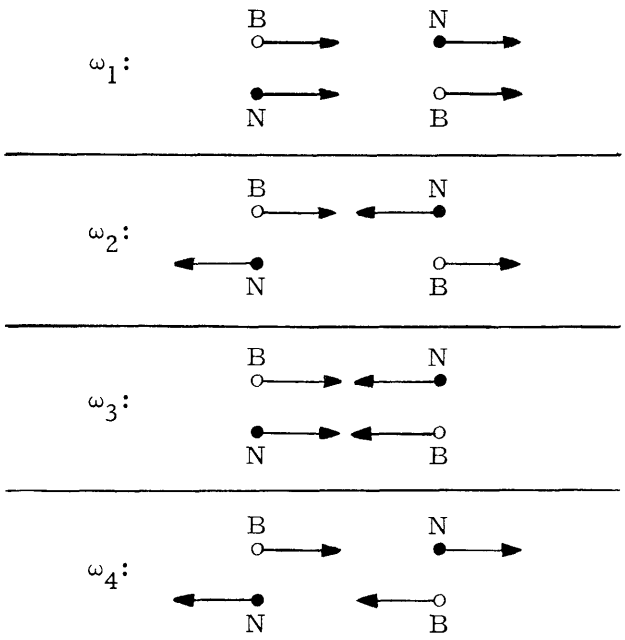

Since our experimental results agree qualitatively with the conclusions from these model considerations for the limit of very small interaction between the planes, we have to assume that these forces are indeed small. Thus the second Raman line will have a rather low frequency and could not be found under the conditions of a relatively broad Raleigh line. With better samples and a laser as the Raman source, it might be possible to find this line.

The interpretation of 2-phonon peaks is mostly done in terms of averaged phonon frequencies for the edge of the Brillouin zone. If we assume the following averaged phonon frequencies for BN

$A = 240\ cm^{-1}$ (acoustical phonon or 2nd Raman active branch)

$O_1 = 680\ cm^{-1}$ (optical phonon, out-of-plane motion)

$O_2 = 1300\ cm^{-1}$ (optical phonon, in-plane motion)

$O_3 = 1300\ cm^{-1}$ (optical phonon, in-plane motion),

the 2-phonon peaks are interpreted as follows:

$920\ cm^{-1}$ $A + O_1$

$1540\ cm^{-1}$ $A + O_2$, $A + O_3$

$2600\ cm^{-1}$ $O_2 + O_3$.

6. Acknowledgments

The authors wish to acknowledge the help of Dr. G. Rupprecht, Tyco Laboratories, Waltham, Massachusetts, in providing the samples. The x-ray studies, the infrared absorption measurements, and the measurement of the dielectric constant were also done at Tyco Laboratories.

R. Geick, C. H. Perry

References

1. R. W. G. Wyckoff, Crystal Structures (Interscience Publishers, Inc., New York, 1960), Vol. I, Chap. III.
2. W. G. Spitzer, D. A. Kleinman, and D. Walsh, Phys. Rev. 113, 127 (1959); T. Deutsch, J. Appl. Phys. 33, 751 (1952).
3. O. Hassel, Norsk. geol. Tidsskr. 9, 258 (1926).
4. A. Brager, Acta physicochim. (U.S.S.R.) 7, 699 (1937) and 11, 617 (1939).
5. R. S. Pease, Acta Cryst. 5, 536 (1952).
6. R. Geick and C. H. Perry, Quarterly Progress Report No. 77, Research Laboratory of Electronics, M.I.T., April 15, 1965, pp. 41-48.
7. A. S. Barker and J. J. Hopfield, Phys. Rev. 135A, 1732 (1964).
8. G. F. Koster, Solid State Physics 5, 173 (1957).
9. R. Loudon, Advances in Physics 13, 423 (1964).

C. CLASSICAL DISPERSION ANALYSIS OF CUBIC PEROVSKITE FLUORIDE CRYSTALS

1. Introduction

Some knowledge of the nature of interatomic forces of cubic fluoride perovskite crystal structures can be determined by a study of the reflection spectra of these crystals. Information on such a crystal structure has been given by Hunt, Perry, and Ferguson[1] for $KMgF_3$. Further information on the damping constants and oscillator strengths of the three transverse optical modes of $KMgF_3$ and similar materials can lead to an interpretation of how the three infrared active vibrations interact.

Barker and Hopfield[2] have used a classical dispersion formula on materials such as $BaTiO_3$, and showed that an independent oscillator model does not give as good a fit to the experimental data. A more complicated model in which two of the strongest oscillators interact, by means of an interaction damping term provides a better fit.[3]

The interatomic forces of the crystal structure can also be studied by replacing the Mg ion with suitable ions, such as Nickel, Manganese or Zinc, or by replacing the

Potassium with Rubidium. Mixed crystals of $KMgF_3$ and $KNiF_3$ may explain how the collective oscillation of the two different B ions of the ABO_3 group interact.

2. Experiment

The reflection spectra of crystals of $KMgF_3$, $KNIF_3$, and some mixed crystals of $K\{(a)Mg+(100-a)Ni\}F_3$ have been measured at room temperature from 4000 cm^{-1} to ~10 cm^{-1} by using unpolarized radiation. The crystals were polished flat, but were irregularly shaped, ranging in size from approximately 5/8 in.-1/4 in. diameter surface.

The reflection measurements were taken at an angle of incidence of ~15°. For the frequency measurements from 4000 cm^{-1} to 300 cm^{-1} a Perkin-Elmer 521 grating double-beam spectrophotometer with a Perkin-Elmer reflectance attachment was used. From 4000 cm^{-1} to 700 cm^{-1} the spectrophotometer was allowed to scan continuously. From 700 cm^{-1} to 300 cm^{-1} it was found that when the spectrophotometer scanned continuously the spectrum shifted to lower frequencies, as compared with a spectrum determined by stopping the instrument every 5 cm^{-1} and taking a reflectivity reading. This discrepancy was due to the long time constant of the double-beam instrument, and was particularly noticeable at low reflectivities and rapid changes in slope. The reflectivity in the region from 350 cm^{-1} to 40 cm^{-1} was measured on a Michelson vacuum interferometer with a specially designed reflection attachment.[4] The spectral region from 350 cm^{-1} to 75 cm^{-1} was measured with a 0.25-mil mylar beam splitter, and from 100 cm^{-1} to 40 cm^{-1} a 1.00-mil mylar beam splitter was used. The reflectivity below 40 cm^{-1} was measured on a single-beam vacuum grating spectrometer.[5] A four-line grating was placed at zero order in the spectrometer, and the average reflectivity of all frequencies below 40 cm^{-1} was determined. This provided a good estimate of the reflectivity in this region, since the lowest frequency reststrahlen peak for all the crystals measured appeared above 100 cm^{-1}, and the reflectivity below 40 cm^{-1} was relatively flat. The single-beam vacuum grating spectrometer was also used to help settle uncertainties in the reflectivity when different runs on the interferometer did not exactly reproduce the same intensity spectrum (for example, at the reststrahlen peaks).

The complete relection spectrum for each sample is an average of a number of separate measurements and the maximum deviation is less than 5 per cent.

3. Data Analysis

The reflectivity was analyzed by using the Kramers-Kronig relation.[6] The transformation gave the real and imaginary parts of the complex dielectric constant $\epsilon' = n^2 - k^2$ and $\epsilon'' = 2nk$ (n is the refractive index, and k is the absorption coefficient). From the dielectric constant data the transverse and longitudinal vibrational frequencies, oscillator strengths, and damping constants were determined. Zeros in the real part of the dielectric constant ϵ' occur at the longitudinal vibrational frequency and at the

transverse frequency. The latter frequency also coincides with maximum in the imaginary part of the dielectric constant ϵ''.

The damping constant is the linewidth at half-height of ϵ'' at the transverse optical mode. The oscillator strength is defined as $S_j = \sqrt{\omega_{t_j} \gamma_j \epsilon''_j}$, where ω_{t_j} is the transverse vibrational frequency, and γ_j is the damping constant. By treating the interaction of electromagnetic waves and the crystal lattice classically, the classical dispersion formula can be written for the complex dielectric constant as a function of the frequency[3]

$$\epsilon(\omega) = \epsilon_\infty + \sum_j \frac{S_j^2}{\omega_j^2 - \omega^2 + i\omega\gamma_j} = \epsilon' + i\epsilon'' = (n^2 - k^2) + i(2nk),$$

where ϵ_∞ is the dielectric constant at high frequencies.

By using the value obtained from the Kramers-Kronig analysis for the transverse vibrational frequency, damping-constants, oscillator strengths, and high-frequency dielectric constant as a first approximation, the relation between the optical constants n and k, and the reflectivity

$$R = \frac{(n-1)^2 + k^2}{(n+1)^2 + k^2} \qquad \text{(for normal incidence)},$$

the classical reflectivity as a function of frequency can be calculated. Adjustment of the parameters ω_{t_j}, γ_j, S_j, and ϵ_∞ for the best fit to the experimental data was made to determine the constants of the infrared active modes.

4. Discussion

All samples studied are of the cubic perovskite crystal structure. The symmetry species of the normal modes are $4F_{1u}$ and $1F_{2u}$,[1] where $1F_{1u}$ is a translational mode, and the F_{2u} is a forbidden mode in the infrared. The reflectivity of each of the pure crystals studied showed three distinct peaks, in agreement with the assignment of normal modes. In the case of K(50 per cent Mg: 50 per cent Ni)F_3, the higher frequency and middle frequency peaks show structure indicating additional oscillators. Figure IV-6 shows the type of classical oscillator fit that was made to the measured reflectivity for $KMgF_3$, K(50 per cent Mg: 50 per cent Ni)F_3, and $KNiF_3$. Table IV-1 lists the transverse and longitudinal vibration frequencies, oscillator strengths, damping constants, and dielectric constants at the high- and low-frequency limits calculated from the Kramers-Kronig analysis of the measured reflectivity. Table IV-2 shows the same parameter as in Table IV-1 but with adjustment made to give the best fit to the measured reflectivity.

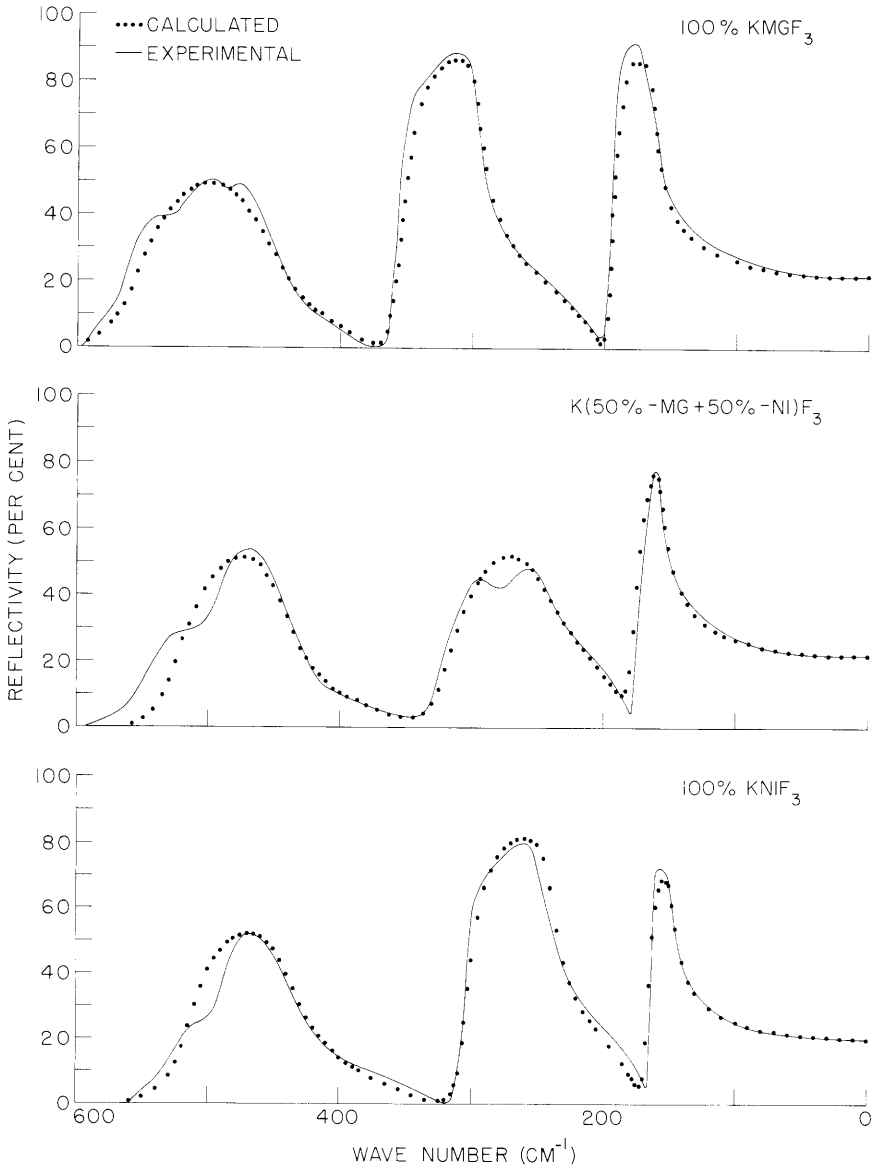

Fig. IV-6. Classical oscillator fit to measured reflectivity.

The classical oscillator fits were made with three oscillators having the frequencies determined from the Kramers-Kronig analysis of the measured reflectivity. The values

Table IV-1. Results of the Kramers-Kronig analysis of the measured reflectivity.

$KMgF_3$				
$\epsilon_o = 7.7$	$\omega_{t_1} = 164$	$\gamma_1 = 8.2$	$S_1 = 320$	$\omega_1 = 198$
$\epsilon_\infty = 2.0$	$\omega_{t_2} = 296$	$\gamma_2 = 10.5$	$S_2 = 372$	$\omega_2 = 359$
	$\omega_{t_3} = 461$	$\gamma_3 = 27.5$	$S_3 = 382$	$\omega_3 = 563$
$K(50\%\ Mg + 50\%\ Ni)F_3$				
$\epsilon_o = 7.7$	$\omega_{t_1} = 155$	$\gamma_1 = 9.2$	$S_1 = 236$	$\omega_1 = 176$
$\epsilon_\infty = 2.1$	$\omega_{t_2} = 249$	$\gamma_2 = 33.5$	$S_2 = 359$	$\omega_2 = 325$
	$\omega_{t_3} = 449$	$\gamma_3 = 25.8$	$S_3 = 380$	$\omega_3 = 544$
$KNiF_3$				
$\epsilon_o = 6.9$	$\omega_{t_1} = 148$	$\gamma_1 = 8.8$	$S_1 = 220$	$\omega_1 = 164$
$\epsilon_\infty = 2.2$	$\omega_{t_2} = 240$	$\gamma_2 = 19.5$	$S_2 = 342$	$\omega_2 = 304$
	$\omega_{t_3} = 439$	$\gamma_3 = 32.0$	$S_3 = 355$	$\omega_3 = 520$

of the transverse vibrational frequencies, together with the oscillator strengths, damping constants, and dielectric constants at the high-frequency limit were varied to achieve the best fit to the measured reflectivity.

No interaction damping was added with the classical fits. We feel that with the addition of some interaction between the highest and middle frequency peak that the fit can be improved.[3]

With the mixed crystals of $KMgF_3$ and $KNiF_3$, a better fit should be obtained with two sets of three oscillators. This is a more difficult case, as the number of parameters is immediately doubled and an initial fit, by using the program of Dr. A. S. Barker, Jr., Bell Telephone Laboratories, Inc., was rather poor and more time will have to be spent on this particular problem.

Table IV-2. Results of a classical oscillator fit with three oscillators and no interaction damping used.

$KMgF_3$			
	$\omega_{t_1} = 164$	$\gamma_1 = 8.2$	$S_1 = 320$
$\epsilon_\infty = 1.90$	$\omega_{t_2} = 296$	$\gamma_2 = 5.9$	$S_2 = 324$
	$\omega_{t_3} = 455$	$\gamma_3 = 40.9$	$S_3 = 338$
$K(50\%\ Mg + 50\%\ Ni)F_3$			
	$\omega_{t_1} = 155$	$\gamma_1 = 9.3$	$S_1 = 236$
$\epsilon_\infty = 2.10$	$\omega_{t_2} = 249$	$\gamma_2 = 33.5$	$S_2 = 375$
	$\omega_{t_3} = 445$	$\gamma_3 = 31.2$	$S_3 = 359$
$KNiF_3$			
	$\omega_{t_1} = 148$	$\gamma_1 = 5.9$	$S_1 = 210$
$\epsilon_\infty = 2.30$	$\omega_{t_2} = 240$	$\gamma_2 = 9.6$	$S_2 = 331$
	$\omega_{t_3} = 439$	$\gamma_3 = 30.7$	$S_3 = 368$

The experimental data of other mixed crystals of $KMgF_3$ and $KNiF_3$, $KMnF_3$, $RbMnF_3$ and $KZnF_3$ have been measured, but the results have not yet been completely analyzed.

We wish to thank Dr. R. Geick for many helpful discussions, and for making appropriate parameter adjustments to the classical dispersion fit whilst visiting the Bell Telephone Laboratories. In this respect, we are indebted to Dr. A. S. Barker Jr. for providing the facilities of his program and cooperation on this problem, and to H. J. Guggenheim, also of the Bell Telephone Laboratories, Inc., Murray Hill, New Jersey, for providing the samples. The Kramers-Kronig analysis and some of the classical dispersion fits were computed at the Computation Center, M.I.T.

C. H. Perry, E. F. Young

References

1. C. H. Perry, Quarterly Progress Report No. 72, Research Laboratory of Electronics, M.I.T., January 15, 1964, pp. 31-38; Phys. Rev. 134, A688 (1964).

2. A. S. Barker and J. J. Hopfield, Phys. Rev. 135A, 1732 (1965).

3. R. Geick and C. H. Perry, Quarterly Progress Report No. 77, Research Laboratory of Electronics, M.I.T., April 15, 1965, pp. 41-48.

4. R. Geick, C. H. Perry, E. C. Reifenstein III, H. D. Wactlar, and E. F. Young, Quarterly Progress Report No. 76, Research Laboratory of Electronics, M.I.T., January 15, 1965, pp. 27-38.

5. C. H. Perry, Quarterly Progress Report No. 70, Research Laboratory of Electronics, M.I.T., July 15, 1963, pp. 19-31.

6. C. H. Perry and B. N. Khanna, Quarterly Progress Report No. 71, Research Laboratory of Electronics, M.I.T., October 15, 1963, p. 25.

D. TEMPERATURE DEPENDENCE OF THE RAMAN SPECTRUM OF $BaTiO_3$

1. Introduction

The Raman spectrum of polycrystalline $BaTiO_3$ has been observed in the Stokes region from 50-1000 cm^{-1} frequency shift from the 22,938 cm^{-1} mercury exciting line over the temperature range 4-475°K. The room-temperature Raman spectrum has been measured by two previous workers[1,2] but their data do not agree with our results or with those of each other. $BaTiO_3$ is of particular interest for Raman measurements, since the lattice symmetry changes as the temperature is lowered from the paraelectric state through the transition temperature to the ferroelectric state and this leads to corresponding changes in the spectrum. This situation becomes more complex as the temperature is lowered and the crystal passes through more first-order changes. Most of the frequencies are in reasonable agreement with the observed infrared[3-5] and neutron data.[6,7] A band at ~310 cm^{-1} has been assigned as the degenerate infrared inactive mode in the cubic state. A strongly temperature-dependent vibration (varying in the range 230-270 cm^{-1}) has been interpreted as the longitudinal mode associated with the low-frequency transverse ferroelectric "soft" mode. This transverse mode could not be observed because presumably it was hidden under the broad Rayleigh line (under the assumption of a value of less than 30 cm^{-1} from the infrared data[5]). No significant temperature dependence of the second-order Raman spectrum in the cubic state could be observed because the bands disappeared rapidly as the temperature was raised above the Curie temperature.

2. Experimental

Irregularly shaped single-crystal samples of $BaTiO_3$, approximately 10 mm long, were studied by means of a Cary Model 81 Raman spectrophotometer. These were grown by a top seeded solution growth technique and had a very pale green coloration. The 4358 Å mercury e-line (22,938 cm^{-1}) was used for excitation in all cases, and the results

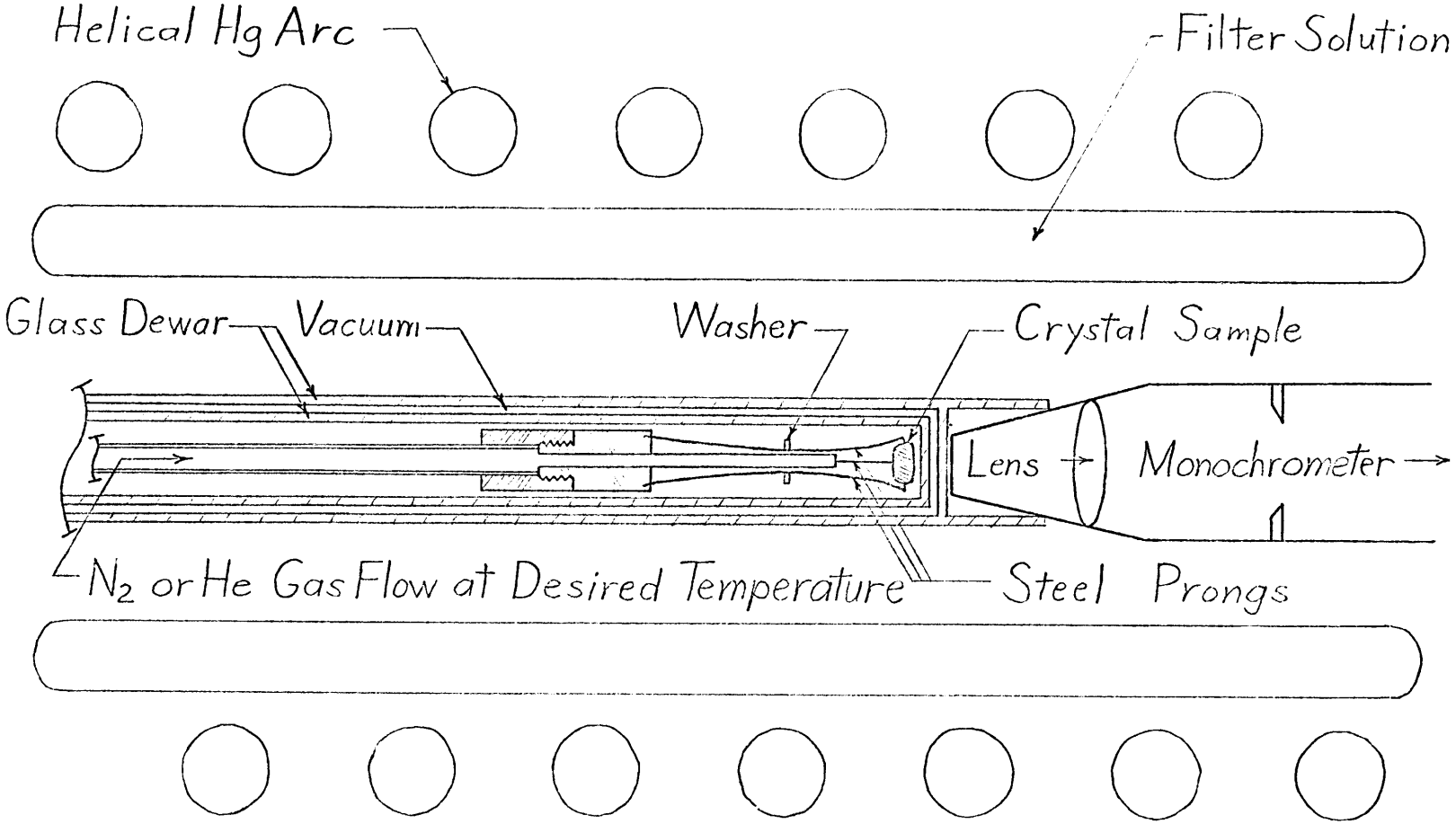

Fig. IV-7. Sample arrangement for studying the Raman effect as a function of temperature.

at room temperature were checked independently by David C. Nelson, of the Applied Physics Corporation, Monrovia, California, who used a duplicate instrument. A very poor Raman spectrum was obtained by using crystals grown by the Remeika method, as these had a slight yellow-brown color, and this approach was discontinued owing to the vastly improved Raman spectrum obtained from the solution-grown samples. No particular orientation of the crystal was chosen and no polarized measurements were taken. A specially constructed double-walled glass vacuum jacket was used for both cooled and heated measurements. The Raman spectrum above room temperature was obtained by using preheated nitrogen gas that was caused to flow through a transfer tube and around the sample (see Fig. IV-7). A calibrated copper-constantan thermocouple attached to the sample was used to measure the temperature, and the temperature was controlled to ±1 °K for the duration of a spectrum. This arrangement was repeated from room-temperature down to liquid-nitrogen temperatures with the same precision by controlling the flow of gas exchanging in a coil immersed in liquid nitrogen. Helium temperatures were obtained by screwing the sample holder into the end of a vacuum-jacketed transfer tube and continuously transferring liquid helium from a storage vessel. Sufficient overpressure in the liquid-helium container provided liquid helium right up to the sample, and the constant temperature was monitored by using a carbon resistance thermometer placed beside the sample. No scattering effect attributable to the liquid-helium droplets was observed. The transfer tube and sample arrangement in the vacuum jacket allowed rapid sample changing, and liquid-helium temperatures could be obtained after only 2 minutes of transferring.

Figure IV-8 shows the Raman spectrum of $BaTiO_3$ as the temperature increases from 5 °K to 473 °K. The relative intensity of all of the graphs is linear and the scale is the same for all of them. Each one of the graphs is an average from as many as 6 runs made at a given temperature.

The lowest run shown in Fig. IV-8 illustrates the gradual change from the first-order tetragonal spectrum of $BaTiO_3$ to the complete disappearance at high temperatures in the cubic phase. High temperatures tend to reduce intensity in general,but, even so, it still appears that $BaTiO_3$ has no second-order spectrum in the paraelectric cubic phase at temperatures sufficiently higher than the Curie point.

Figure IV-9 shows the strong temperature dependence of the most intense peak indicated in the previous graphs. Especially noticeable are the discontinuities at the two transition points, and the peak was never observed at an intermediate value. Figure IV-10 shows 5 runs, going first up and then down in temperature through the rhombohedral-orthorhombic phase transition region. Going up, the change is between 190 °K and 198 °K; going down, the change is between 190 °K and 182 °K. The graphs in this figure were traced directly from one of the runs on the recorder paper, with the fluctuations caused by noise smoothed out. The same run was made 3 or 4 times with

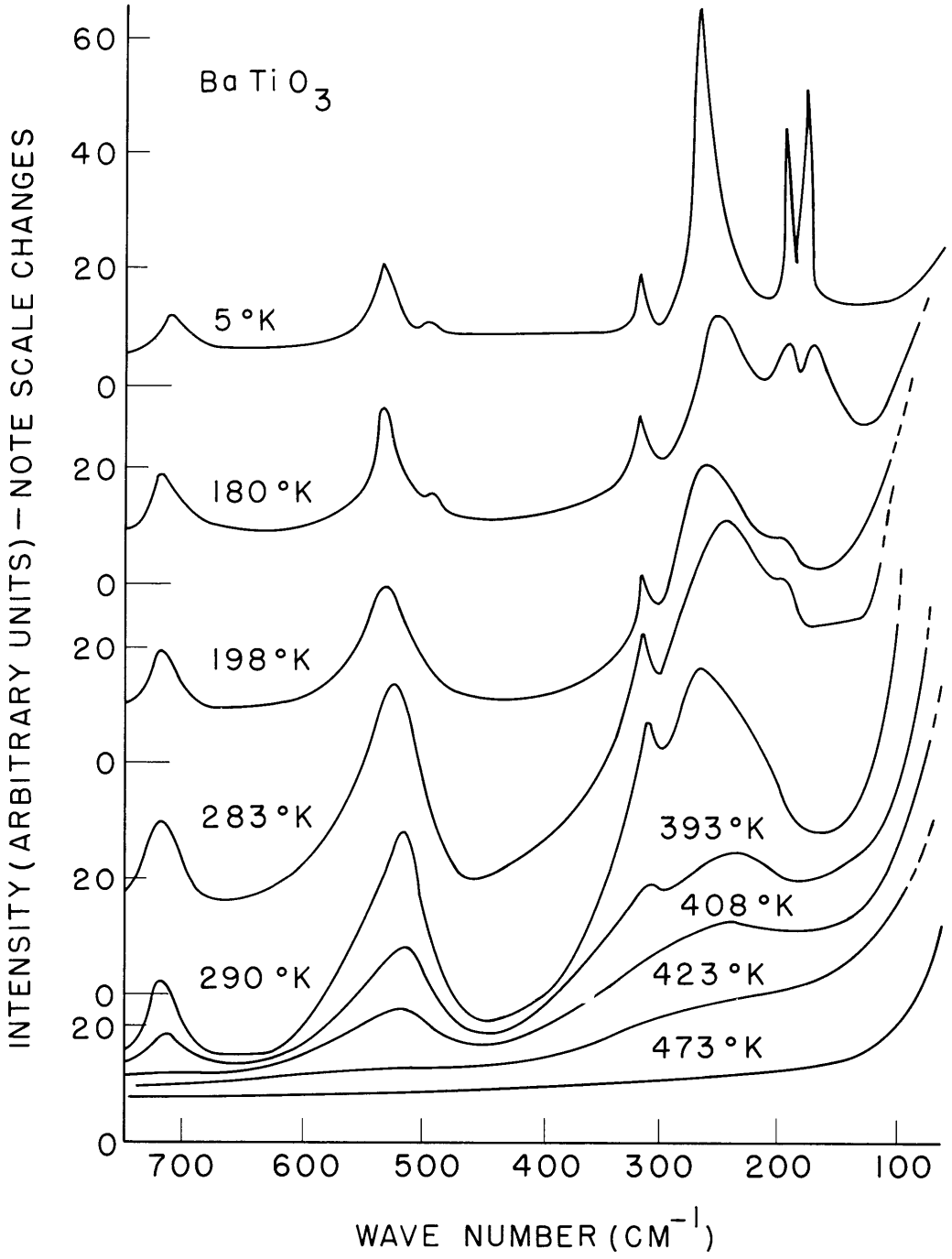

Fig. IV-8. Raman spectrum of $BaTiO_3$ from 5°K to 473°K.

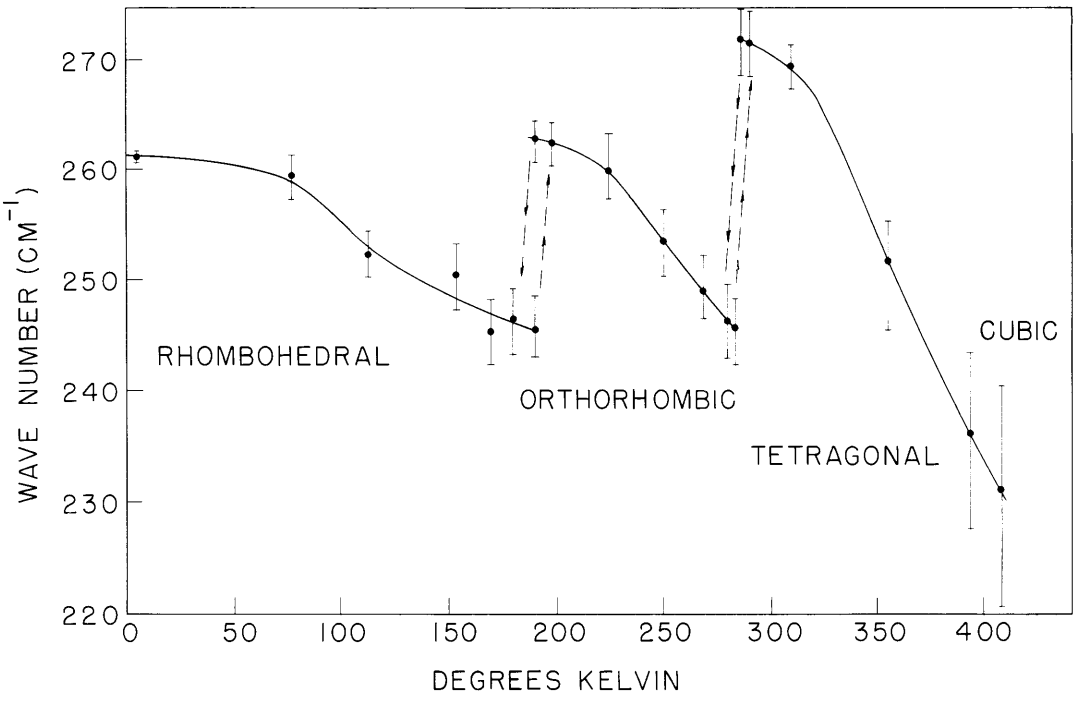

Fig. IV-9. 270-cm^{-1} room-temperature peaks vs temperature.

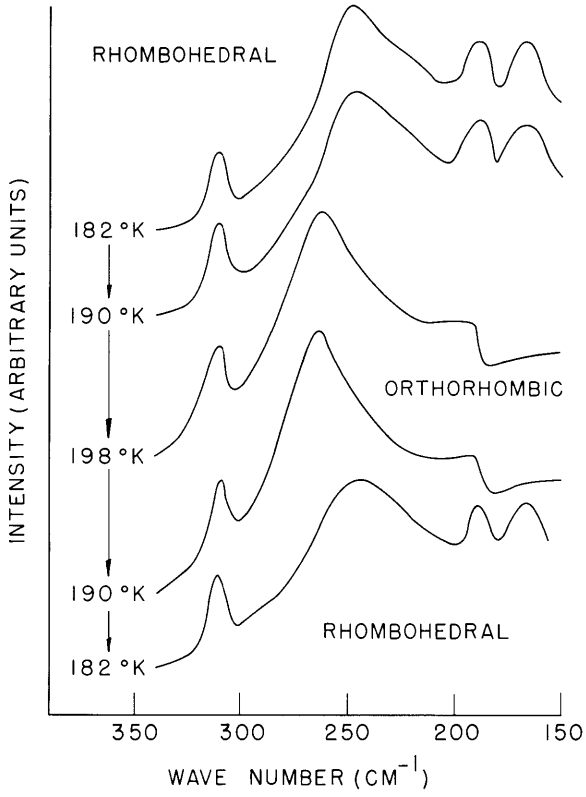

Fig. IV-10.
Hysteresis effect in the rhombohedral-orthorhombic transition.

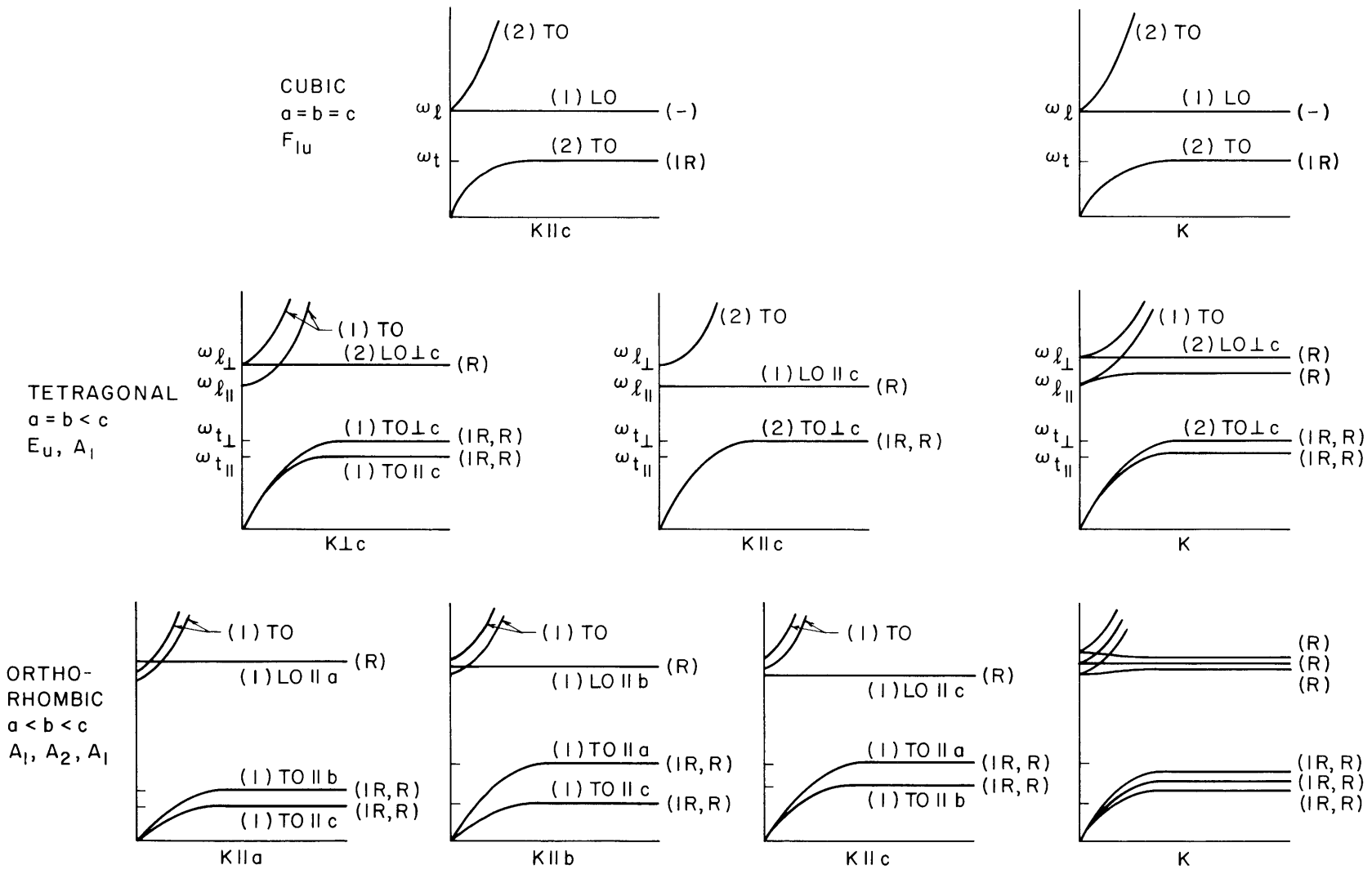
CUBIC
a = b = c
F_{1u}
ω_ℓ
ω_t
(2) TO
(1) LO
(-)
(2) TO
(IR)
K ∥ c
K
TETRAGONAL
a = b < c
E_u, A_1
$\omega_{\ell\perp}$
$\omega_{\ell\parallel}$
$\omega_{t\perp}$
$\omega_{t\parallel}$
(1) TO
(2) LO ⊥ c
(R)
(1) TO ⊥ c
(IR, R)
(1) TO ∥ c
(IR, R)
K ⊥ c
(2) TO
(1) LO ∥ c
(R)
(2) TO ⊥ c
(IR, R)
K ∥ c
(1) TO
(2) LO ⊥ c
(R)
(R)
(2) TO ⊥ c
(IR, R)
(IR, R)
K
ORTHO-
RHOMBIC
a < b < c
A_1, A_2, A_1
(1) TO
(1) LO ∥ a
(R)
(1) TO ∥ b
(IR, R)
(1) TO ∥ c
(IR, R)
K ∥ a
(1) TO
(1) LO ∥ b
(R)
(1) TO ∥ a
(IR, R)
(1) TO ∥ c
(IR, R)
K ∥ b
(1) TO
(1) LO ∥ c
(R)
(1) TO ∥ a
(IR, R)
(1) TO ∥ b
(IR, R)
K ∥ c
(R)
(R)
(R)
(IR, R)
(IR, R)
(IR, R)
K

(a)

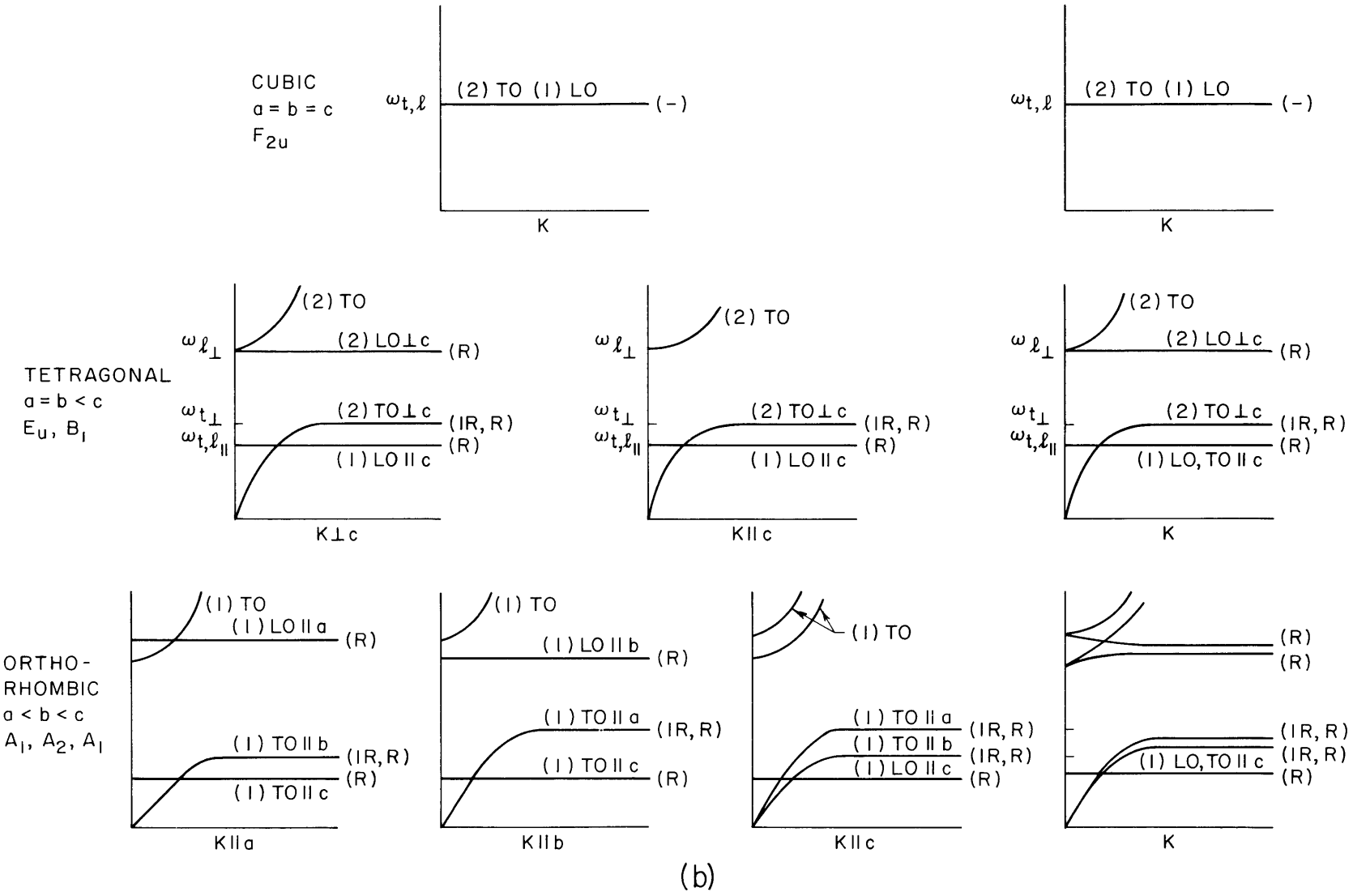

Fig. IV-11. Phonon dispersion curves at small-wave vector k.

the same results. After examining all of the data, the rhombohedral-orthorhombic transition region was limited to an 18°K range, and the orthorhombic-tetragonal region was confined to a 7°K range. More accurate work will have to be done to detect hysteresis in the 7°K range.

3. Discussion

The long-wavelength lattice vibrations of a polar diatomic lattice having cubic symmetry have been treated by Huang.[8] Loudon[9,10] extended the dynamical theory to uniaxial crystals and showed that the frequencies of the Raman active phonons are determined by a quadratic equation in ω^2 having two distinct roots so that

$$\omega^2 = \omega_{t_{||}}^2 \sin^2\theta + \omega_{t_\perp}^2 \cos^2\theta \tag{1}$$

$$\omega^2 = \omega_{\ell_{||}}^2 \cos^2\theta + \omega_{\ell_\perp}^2 \sin^2\theta, \tag{2}$$

where $\omega_{t_{||}}$ and $\omega_{\ell_{||}}$ are the transverse and longitudinal optical modes, respectively, parallel to the c-axis, and $\omega_{t_\perp}$ and $\omega_{\ell_\perp}$ are the transverse and longitudinal modes, respectively, perpendicular to the c-axis, and θ is the relative orientation of the phonon wave vector $\underline{k}$ and the c-axis. These characteristic frequencies are based on the assumption that $\epsilon_{||} - \epsilon_\perp$ is small, that is, $\left|\omega_{t_{||}} - \omega_{t_\perp}\right| \ll \omega_{\ell_{||}} - \omega_{t_{||}}$, and $\omega_{\ell_\perp} - \omega_{t_\perp}$.

No work has been reported for a biaxial crystal, and the frequencies of the three Raman-active phonons are determined by a cubic equation in ω^2 and all will vary with the direction of propagation. This theory ceases to be valid when there is more than one group of 3 lattice vibrations in infrared-active phonons, although the generalizations of the Cochran and Cowley[11] extensions of the Lyddane-Sachs-Teller relationship,

$$\prod_{j=1}^{N} \left[\frac{\omega_\ell(j)}{\omega_t(j)}\right]^2 = \frac{\epsilon_o}{\epsilon_\infty},$$

continue to apply. Provided that the groups of infrared active phonons are well separated, the variations of their frequencies with θ, say, for the tetragonal form may still be represented by Eqs. 1 and 2, and this is assumed to be the case for $BaTiO_3$.

For $BaTiO_3$ the paraelectric crystal symmetry is O_h^1 with 5 atoms per unit cell situated at centers of inversion, leading to $3F_{1u}$ infrared-active modes and one F_{2u} "silent" mode.

Figure IV-11 shows the phonon dispersion curves at small-wave vector for which electrostatic forces predominate over anisotropy in the interatomic forces; included are the various branches for the cubic tetragonal and orthorhombic forms. The

Table IV-3.

(a) Raman Frequencies (cm^{-1})

Structure	T°K	ν_4(LO)	ν_4(TO)	$\nu_3\left(\frac{LO}{TO}\right)$	ν_1(LO)	ν_2(TO)		ν_1(TO)
Rhombohedral	5	712	530 (488)	311	261	189	174	
	113	718	528 (490)	312	252	188	170	
	180	717	528 (489)	311	246	189	168	
Orthorhombic	198	717	526	310	262	(195)		
	249	718	523	309	253	(195)		
	283	718	519	309	245	(195)		
Tetragonal	290	722	518	307	271			
	310	720	516	306	269			
	355	720	511	307	250			
	393	718	512	306	235			
Cubic	408	–	515	–	230			
	473	–	–	–	–			

(b) Infrared Frequencies (cm^{-1})

Rhombohedral			530 (490)					
Orthorhombic			520 (495)					
Tetragonal			517 (495)					
Cubic[3]			495			340*		225 (calc.)
Tetragonal[4]			491			183		33
Tetragonal			491			184	175	15
Cubic[5]			491			184		15

(c) Neutron Frequencies (cm^{-1})

Tetragonal	301	780	450			350 (sharp)		235
Cubic[6]	423	780	450			350 (broad)		235
Cubic[7]†	423	780	450	235				
Our Interpretation	423	780	450	340	235			

*This band found by Last[3] has been shown not to exist in the infrared spectrum by both Spitzer[4] and Ballantyne.[5]

†Lefkowitz[7] has suggested that the 340-cm^{-1} band is a surface impurity on the basis of the nonexistence of this band in the infrared. The appearance of bands in the neutron spectrum do not depend on their infrared activity.

polycrystalline nature of our samples and the predominance of electrostatic forces over the anisotropy ensure that the departures of the branches in most cases will be small. The Raman data essentially agree with these predictions and it is only at low temperatures that some of the splittings can be observed. No splittings are observed at any temperature for the F_{2u} mode but presumably below the Curie temperature the crystal is just sufficiently distorted from the cubic form for the mode to be Raman-active.

Table IV-3 summarizes the results and our interpretations The data at different temperatures have been listed, together with the measured infrared[3-5] and neutron data.[6,7] The agreement is quite good and we feel that Pelah and Lefkowitz' original interpretation[6] is better than the later comments made by Lefkowitz[7] with respect to their 340-cm^{-1} band. We have interpreted this band as the "silent" mode in the cubic material, as there is no corresponding band in the infrared.[5] The strongly temperature-dependent peak is probably the longitudinal vibration associated with the ferro-electric mode observed by Ballantyne[5] at 12 cm^{-1}. Using the modified Lyddane-Sachs-Teller relationship[11] and assuming $\nu_{2_T} \approx \nu_{2_L}$, we obtain a value of ~16 cm^{-1} for the ν_{1T} "soft" mode with our Raman frequency data very close to the Curie temperature. This also adds to the credibility of the assignment, although the unusual temperature dependence is probably sufficient justification.

The addition of new bands at low temperatures is probably the result of mode splitting arising from the temperature effect that sharpens the peaks and the distortion of the material from the "cubic" form.

We would like to thank Dr. A. Linz, of the Materials Center for Science and Engineering, M.I.T., for the samples, Dr. J. Ballantyne, of the Electrical Engineering Department, Cornell University, for his interest and collaboration in the initial stages of this work, and Mr. D. C. Nelson, of the Applied Physics Corporation, for confirming our results at room temperature.

D. B. Hall, C. H. Perry

References

1. Ya. S. Bobovich and E. V. Bursian, Opt. i Spektroskopiya 11, 131 (1961).
2. S. Ikegami, J. Phys. Soc. Japan 19, 46 (1964).
3. J. T. Last, Phys. Rev. 105, 1740 (1957).
4. W. G. Spitzer, R. C. Miller, D. A. Kleinman, and L. E. Howarth, Phys. Rev. 126, 1710 (1962).
5. J. M. Ballantyne, Quarterly Progress Report No. 73, Research Laboratory of Electronics, M.I.T., April 15, 1964, p. 13.
6. I. Pelah and I. Lefkowitz, Proc. Symposium on Inelastic Scattering of Neutrons in Solids and Liquids, Vienna, 1960.
7. I. Lefkowitz, Proc. Phys. Soc. (London) 80, 868 (1962).
8. K. Huang, Proc. Roy. Soc. (London) A 208, 352 (1951).

9. R. Loudon, Proc. Phys. Soc. (London) 82, 393 (1963).
10. R. Loudon, Advances in Physics 13, 423 (1964).
11. W. Cochran and R. A. Cowley, J. Phys. Chem. Solids 23, 447 (1962).